RSC Advances

ROYAL SOCIETY OF CHEMISTRY

www.rsc.org/advances

Fabrication of superhydrophobic graphene surface with excellent mechanical abrasion and corrosion resistance on aluminum alloy substrate

Yan Liu[a,*], Jijia Zhang[a], Shuyi Li[a], Yaming Wang[b], Zhiwu Han[a], Luquan Ren[a]

a.Key Laboratory of Bionic Engineering (Ministry of Education), Jilin University, Changchun 130022, China; b.Institute for Advanced Ceramics, Harbin Institute of Technology, Harbin 150001, China

Abstract: A superhydrophobic graphene film with excellent mechanical abrasion resistance and corrosion resistance was successfully deposited on Al alloy by spin-coating method. The surface structure morphology, chemical composition, wettability, mechanical abrasion and corrosion resistance were characterized by means of scanning electron microscopy, atomic force microscopy (AFM), Fourier-transform infrared spectrophotometer, X-ray photoelectron spectroscopy, water contact angle measurements, wear tester and electrochemical workstation. It was found that the static water contact angle on the as-prepared surface was as high as 153.7 ± 2°. Furthermore, the as-prepared surface exhibited excellent mechanical abrasion resistance and corrosion resistance, which were studied by Tafel curve and electrochemical impedance spectroscopy (EIS). It is expected that this simple and versatile methodology for preparing a graphene-reinforced coating can open a new avenue especially for multi-functional engineering materials and be conveniently extended to other metal substrates.

KEYWORDS: Graphene, Superhydrophobicity, Mechanical abrasion, Corrosion

* Corresponding author. Tel.:+86 431 85095760; fax:+86 431 85095575
E-mail address:liuyan2000@jlu.edu.cn

resistance

Introduction:

In recent years, more and more researchers have paid close attention to fabricating superhydrophobic coatings on the surface of various metal materials.[1-7] Amongst different metal materials, aluminum (Al) alloy exhibits superior properties, such as low density, excellent thermal and electrical conductivity, high specific strength and good castability. However, the surface of Al alloy is easily corroded by Cl^- in neutral aqueous solutions.[8] To prolong the lifetime of Al alloy, corrosion protection is important due to the widespread use of these materials in structural, marine, and aerospace applications.[9-11]

Recently, a new class of two-dimensional carbon nanostructure named graphene has triggered unprecedented research excitement.[12] Graphene has been developed to build hydrophobic films these days.[13,14] Graphene has superior characteristics such as high electrical conductivity,[15-17] outstanding carrier mobility[18,19] and splendid optical transmittance in the visible regime (up to 97.73%),[20-23] excellent chemical inertness, thermal stability,[24] high mechanical strength,[25-28] etc. Possessing the outstanding performance, graphene has potential as an ultrathin protective coating especially in protection of metals from oxidation and corrosion in marine or saline environment. In fact graphene forms a natural diffusion barrier providing a physical separation between the protected metal and reactants.[29] Some investigators[30–33] have developed graphene-based environmental barrier coatings on metal substrates. Several pioneering experiments have demonstrated that single-layer and multi-layer graphene

films can serve as corrosion-inhibiting coatings for Cu and Cu–Ni alloy.[34–38] Zhao[39] transferred monolayer graphene onto the surface of Ag thin film as a transparent and ultra-thin protective barrier. He et al.[40] reported electrophoretic deposition of graphene oxide as a corrosion inhibitor for sintered NdFeB. Mayavan et al.[41] demonstrated that Fe surface with the graphene oxide ink coating exhibited improved corrosion resistance in an aggressive chloride environment, which is attributed to the excellent barrier property of graphene. Chang et al.[42] also proved that epoxy/graphene composites could be used as corrosion inhibitor for cold-rolled steel. However, graphene coating with corrosion resistance on Al alloy substrate is rarely discussed.

Based on the above discussions, we hereby report a simple and efficient method to prepare a superhydrophobic graphene coating on Al alloy substrates. The hydrophobicity of the coatings was discussed, and the corrosion behavior of the superhydrophobic coating on Al alloy was explored. Meanwhile, the wear performance of the surfaces was also investigated.

Experimental

Preparation of graphene nanosheets

In a typically improved Hummer's method, (graphene oxide) GO was synthesized by oxidation of 3.0 g natural graphite flake (325 mesh; Tianjin, China) using $KMnO_4$ (18.0 g) in mixture of (98%) H_2SO_4/(85%) H_3PO_4 (360 mL:40 mL). The GO powder was then heated to 50 °C and stirred for 12 h. After cooled to room temperature, the powder was poured onto the ice (400 mL) with 30% H_2O_2 (3 mL).The obtained mixture was filtered and washed in 10% aqueous HCl solution and deionized (DI)

water to remove the acid. For further purification, we carried out dialysis for 1 week. At last the powder was centrifugated at a speed of 11000 rpm for several times using a High speed centrifuge (An Hui USTC Zonikia Scientific Instruments Co. Ltd), and dried using a vacuum freeze-drying technology. All the chemicals and materials were used without any further purification. GO was firstly dispersed in distilled water using an Ultrasonic Cell Crusher to create a 1 mg/ml GO dispersion. Then 42.5 ml of 80% hydrazine monohydrate was added to 60 ml of the GO dispersion. After being vigorously shaken or stirred for a few minutes, the mixture was treated in an oil bath (50℃) for 12 h. The obtained black dispersion was then subjected to centrifugation for 30 min at 11000 rpm. Then the obtained graphene was washed with anhydrous ethanol and dried at 50℃ in a vacuum oven.

Preparation of graphene coatings

The composition of the 2024 Al alloy used was 4.2 wt.% Cu, 1.5wt.% Mg, 0.7 wt.% Mn, 0.2 wt.% Fe, bal. Al. The Al alloy specimens were cut into samples with a size of $15 \times 15 \times 1$ mm^3. The samples were polished with silicon carbide papers (from 400 to 800 grades) to remove the oxide on the surfaces, cleaned in anhydrous ethanol for 10 min, and dried in turn. In order to disperse the graphene sheets, we performed high-power ultrasonication to the graphene powder in anhydrous ethanol to obtain homogeneous 0.2 mg/ml black graphene suspensions. To deposit the graphene film, 10 cm^3 of the suspension was gently released on the Al alloy substrate by spin coating and allowed to dry for 12 h in a vacuum oven to evaporate the solvent. The samples were photographed with a digital camera (Sony Ltd., Japan). Static water contact

angles of the fabricated surfaces were measured with a contact angle meter (JC2000A Powereach, China) based on a sessile drop measuring method with a water drop volume of 3 μL. The samples were measured at five or more different positions and the CAs were averaged. The surface morphology of GO coated Al alloy was examined by a field emission scanning electron microscope (SEM, EVO 18, ZEISS). The chemical components of different samples were recorded at room temperature on Fourier-transform infrared spectrophotometer (FTIR, JACSCO, Japan) and X-ray photoelectron spectroscopy (XPS, ESCALAB 250Xi).

Frictional and Wear Performance Test

The coated specimens were cut into samples with a size of 15 × 15 × 1 mm^3 for the friction and wear test. Wear resistance of the samples was examined by Universal Micro-Tribometer (CETR, America) at room temperature, one reciprocation motion type. 45# steel was used as a counterpart (100 × 100 × 3 mm^3). Each test was repeated at least three times. The wear test was performed at 10 N load condition. Test pattern is 60 s wear test. Before each test, the surface of the 45# steel was polished to a roughness of about 0.1 mm, and all the specimens were ultrasonically cleaned in anhydrous ethanol and dried before and after wear tests. The mass loss was measured by a sensitive electronic balance with an accuracy of 0.0001 g. To assist the analysis of wear mechanisms, the worn surfaces of block specimens were examined by scanning electron microscopy (JSM-5600LV, Japan). The hardness was measured by using a FM-700 Vickers hardness tester with 200 g load and a dwell time of 15 s.

Electrochemical experiments

The electrochemical measurements were carried out in a three electrode cell. The electrochemical cell involves three electrodes: a superhydrophobic graphene coating on Al alloy with an area of 1 cm^2 exposed was used as the working electrode, a platinum plate as the counter electrode, and a saturated calomel electrode (SCE) as the reference electrode. All measurements were performed on electrochemical analyzer (CHI604E, China) in 3.5 wt.% NaCl solution at room temperature (25℃). For Tafel experiments, the potential was scanned at a rate of 10 mV/s. EIS measurements were carried out at open circuit potential with an AC amplitude of 5 mV over a frequency range of 0.01 Hz – 10 kHz. Each electrochemical test was carried out at least three times to ensure reproducible results.

Result and discussion

Superhydrophobic graphene coatings on Al alloy

The graphene oxide dispersion was spin-coated on Al alloy substrate. SEM image was used to evaluate the structure of GO coating in Fig. 1. We can discover that GO was coated uniformly on Al alloy substrate. The schematic representation of superhydrophobic graphene fabricated and its coating on the Al alloy is shown in Fig. 2.

GO was sonicated in different solvents to reduction including water, alcohol and acetone. The CAs of graphene films prepared by different solvents and the shapes of water droplet on an Al alloy substrate are shown in Fig. 3. Al alloy (2024Al) is intrinsically a hydrophilic engineering material with a native oxidized layer that has an average water contact angle of 67.1 ± 1°. When graphene sonicated in acetone

(Graphene-A) was deposited on the Al alloy substrate, the coated 2024Al alloy surface exhibited high hydrophobicity with an average water contact angle of about 125.3 ± 1°. The water contact angle of the Al alloy substrate with Graphene-E coating was the highest value. The opposite effect was observed with graphene sheets being sonicated in water (Graphene-W). The water contact angle of the Al alloy substrate with Graphene-W coating was observed to exhibit superhydrophilicity (2.2° ± 1°), as shown in Fig.3. In the process of drying for different samples, acetone and ethanol evaporated quickly, leaving the graphene on the surface. However, the vapour tension of water is much higher than that of either acetone or ethanol, so water might not have been completely evaporated from the coating, which may be the main reason for a low CA 2.2 ± 1°. Furthermore, the inset in Fig. 3 shows the shapes of water droplets with 20μL on Graphene-E coated Al alloy under tilt angle of 0 and 180. It is seen that the water droplet keeps a steady spherical shape and it is pinned to the surface even when the substrate is turned upside down. We deposited increasing volume of water droplet on the superhydrophobic surface and it was turn out that droplet was not dropped down the until the droplet was up to 50μL, which proves the highly adhesive nature of graphene coating.

To explain why the differences for acetone and ethanol are so big, XPS analysis has been performed on four samples and the C1s spectrum is shown in Figure. 4. The broad C1s peak of four samples can be fitted into 2 peaks with the binding energy at 284.7 and 287.4 eV, corresponding to the C-C, C=O, respectively. It can be seen that the GO has significant peak at 287.4 eV, whereas for the other three samples the

group can be barely observed. The peak intensity of C=O decreased after chemical reduction, and peak intensity C-C for Graphene-E is the highest. Accordingly, the ratio of O1s to C1s is decreased significantly, for Graphene-E, the ratio is the lowest. For Graphene-E, we consider the Wenzel model to explain the excellent performance. The coating enhances the surface roughness of the Al Alloy substrate.

In the Wenzel model, the contact angle on a rough surface in the homogeneous regime θ_w, the Equation is：

$$\theta_w = r\cos\theta$$

θ represents the contact angle on the flat surface and r is the roughness ratio. r is usually larger than 1. When a water drop falls on the surface of Graphene-E coating, as an individual Graphene-E nanosheet exhibits hydrophobicity (θ>90°), θ_W will be larger than 90°. The more the Graphene-E nanosheets, the larger θ_W will be, then the Wenzel model indicates that a rough Graphene-E coating shows superhydrophobicity.

To better understand why Graphene-E coating is superhydrophobic, we performed reflectance-mode Fourier transform infrared (FTIR) spectroscopy measurements on GO and Grahene-E produced in this study, as is shown in Fig. 5. The FT-IR spectrum of GO clearly shows the following characteristic peaks: GO exhibits typical absorption features of the coupled C-O stretching vibrations at 1051 cm^{-1}, C=O stretching vibrations at 1641 cm^{-1}, CH_2, CH_3 stretching vibrations at 2854, 2922 and 2972 cm^{-1}. The disappearance and weakness of the oxygen functional group peaks of Graphene-E nanosheets, compared to original GO, strongly demonstrated the reduction of GO.

At last, the Graphene-E coating has been characterized by atomic force microscopy (AFM) in Fig. 6. Fig. 6 shows AFM images and surface roughness values of multilayer graphene coating. The surface roughness of the coating is 6.24 nm (RMS value).

Combining the above analysis of different samples, we can conclude that the superhydrophobicity of Graphene-E may be both attributed to the different chemical components and the surface roughness of graphene coating.

Wear Mechanisms of the Coatings

Generally, the wear-resistance of coating could be improved with an increase in hardness. From the tests and statistics of the hardness values of coatings, the following results can be obtained: the hardness values of Al alloy substrate is mostly concentrated in a range of 60~80 Hv，whereas the hardness values of the graphene is mainly distributed in a range of 90~100 Hv. This implies that the coating increases the hardness values of the Al alloys to a certain extent.

The worn surfaces generated by different wear conditions have quite different characteristics, so their wear mechanism can be discussed through analyzing the morphology of the worn surface. Fig. 7 shows the SEM micrographs of the worn surface of the bare Al alloy and the Graphene-E coated Al alloy. Fig. 7a demonstrates the worn surface of the bare Al alloy. As a comparison, in Fig. 7b shows SEM photograph of the worn surface of coated Al alloy. In Fig. 7a, the grooves in SEM images were greater and deeper, while grooves in the coated Al alloy in Fig. 7b were less and smaller. It was noted that the worn surface of the coated Al alloy was

characterized by slight spalling, cutting damage and grooves on the graphene coating under a load of 10 N, with adhesive wear being the major wear form. However, the worn surface of the pure Al alloy has severe spalling and typical adhesive wear appears. Generally, severe adhesive wear easily causes massive mass loss of materials and wear life can decrease apparently.

Electrochemical measurement and corrosion behavior

In order to determine how to protect an active metal from corrosion, the fundamental aspects of degradation must be investigated. When the metal surface is exposed to solution, the local electrochemical cell functions. For the electrochemical reaction of Al, we expect the anodic and cathodic reactions to be as follows:

$Al \rightarrow Al^{3+} + 3e^-$ Anodic reaction

$2H^+ + 2e^- \rightarrow H_2\uparrow$ Cathodic reaction

The only way to inhibit corrosion is to avoid the contact between electrolyte and the cathodic reactant. The main method to prevent such corrosion is using a barrier coating to suppress the cathodic reaction by limiting the diffusion of electrolyte, oxygen and water to the substrate. It also limits the transport of electrons to the metal interface.

Tafel curves analysis

Fig. 8 shows the Tafel polarization curves of bare Al alloy and Graphene-E coated Al alloy (Gr/Al). The ability of the superhydrophobic coating to protect Al alloy from corrosion in 3.5 wt.% NaCl solution was studied by electrochemical experiments. The difference in the polarization curves between the untreated sample and the

superhydrophobic sample is shown in Fig. 8. The polarization curve of coated Al shows a significant shift of corrosion potential to more positive values (-1452 mV) compared to bare Al alloy (-1329 mV), and the coated samples have much smaller corrosion current density, thereby indicating that coated Al alloy has much better corrosion resistance than bare Al alloy. From the overall results of Tafel plot it can be summarized that the coated film acts as a very strong passivation layer against ion diffusion and corrosion. This can be attributed to the reduced GO coating which acts as a barrier to electron and ion transport between the substrate and the sodium chloride solution.

Table1 summarizes the E_{corr} and i_{corr} of superhydrophobic graphene coated and uncoated Al alloys. The E_{corr} of superhydrophobic graphene coated Al alloy decreases to a less negative value compared to bare Al alloy, indicating a negligible tendency to corrode. Similarly, the i_{corr} of superhydrophobic graphene coated specimen（**2.54×10^{-7} A/cm^2**）is also significantly lower than that of bare Al alloy (**7.19×10^{-4} A/cm^2**).

Electrochemical Impedance Spectroscopy(EIS)

The excellent electrochemical performances of graphene shows that it can be used in a variety of applications such as energy storage and generation applications.[43-45] The electrochemical technique of EIS is also applied for understanding electrochemical degradation of metals and their coated samples. Nyquist plots represent the real component of impedance versus the imaginary component of impedance on a linear scale. The typical Nyquist plots are presented in Fig. 9. For the superhydrophobic sample, the impedance semicircle enlarges markedly. The larger diameter curve in the

Nyquist plot for the superhydrophobic sample shows a higher Z' '(real impedance), which means the coating is more capacitive, providing more protection against corrosion,[46,47] but the curve for bare Al alloy barely visible. It is obvious that the corrosion resistance of the coated Al alloy is greater than that of the uncoated Al alloy, which is consistent with the polarization results as shown in Fig. 8.

Bode plots have been selected in this study as the representation of the corrosion resistance due to graphene coating. It is concluded that the corrosion resistance of the graphene coated Al alloy is at least an order of magnitude greater than that of the uncoated Al alloy as shown in Fig. 10a. The observed behaviors can be understood by fitting the data to simple equivalent circuit models. The phase angle plots indicate the presence of two time constants as shown in Fig. 10b.

For a more quantitative insight into the electrochemical phenomena that leads to this improvement, electrical equivalent circuits (EEC) were employed to analyze the impedance data. Fig. 11a shows the equivalent circuit model of the bare Al alloy sample, which represents the electrochemical behavior and shows one time constant. In this equivalent circuit, the electrolyte resistance is represented by Rs. R_1 is the charge transfer resistance, and CPE is the constant phase element. The value of R_1 reveals total corrosion resistance performance. In the case of the electrode protected with the superhydrophobic graphene coating, the equivalent circuit model should consider two time constants, as shown in Fig. 11b. In this EEC, R_s is the solution resistance, R_1 refers to the charge transfer resistance, the coating capacitance is represented by CPE_2, and R_2 is associated with the impedance of the film, while

electrical double layer capacitance is represented by a constant phase element (CPE_1). The superhydrophobic graphene coating acts as a corrosion-inhibiting coating which significantly improves the corrosion resistance of Al alloy as shown schematically in Fig. 12. The Al oxide formed on Al under ambient conditions cannot protect it from corrosion under the influence of chloride ions. On the contrary the graphene coating on Al alloy protects it from electrochemical degradation in an aggressive chloride environment.

Conclusions

A superhydrophobic graphene film with excellent mechanical abrasion and wear resistance has been prepared successfully. The water contact angle is 153.7 ± 2°. The results indicate that the wear resistance of graphene coatings is improved obviously compared to the bare Al alloy substrate, which is attributed to the improved hardness. The analysis of Tafel and EIS reveals that the Al alloy corrosion is effectively inhibited by superhydrophobic graphene coating. The electrochemical technique of EIS reveals that the graphene coating effectively suppresses metal oxidation and oxygen reduction. The superhydrophobic coating has superior corrosion resistance property and can be widely applied to the corrosion protection for various engineering materials.

Acknowledgements

This work was supported by the National Natural Science Foundation of China (Nos. 51275555, 51325501 and 5147200) and and Basically Science Research Foundation of Jilin University (No. 2013ZY09)

References

1 B. Yin, L. Fang, A. Q. Tang, Q. L. Huang, J. Hu, J. H. Mao, G. Bai and H. Bai, *Appl. Surf. Sci.*, 2011, **258**, 580–585.

2 L. Zhao, Q. Liu, R. Gao, J. Wang, W. L. Yang and L. H. Liu, *Corros. Sci.*, 2014, **80**, 177–183.

3 B. T. Qian and Z. Q. Shen, *Langmuir*, 2005, **21**, 9007–9009.

4 H. Liu, S. Szunerits, W. Xu and R. Boukherroub, *ACS Appl. Mat. Interfaces*, 2009, **1**, 1150–1153.

5 C. R. Crick, J. A. Gibbins and I. P. Parkin, *J. Mater. Chem. A*, 2013, **1**, 5943–5948.

6 Z. W. Wang, Q. Li, Z. X. She, F. N. Chen and L. Q. Li, *J. Mater. Chem.*, 2012, **22**, 4097–4105.

7 Q. F. Xu and J. N. Wang, *New J. Chem.*, 2009, **33**, 734–738.

8 W. A. Badawy, F. M. Al-Kharafi and A. S. El-Azab, *Corros. Sci.*, 1999, **41**, 709–727

9 P. C. R. Varma, P. Periyat, M. Oubaha, C. Mcdonagh and B. Duffy, *Surf. Coat. Technol.*, 2011, **205**, 3992–3998.

10 Y. J. Du, M. Damron, G. Tang, H. X. Zheng, C. J. Chu and J. H. Osborne, *Prog. Org. Coat.*, 2001, **41**, 226–232.

11 W. A. Badawy, F. M. Al-Kharafi and A. S. El-Azab, *Corros.Sci.*, 1999, **41**, 709–727.

12 A. K. Geim and K. S. Novoselov, *Nat Mater*, 2007, **6**, 183–191.

13 X. Q. Zhang, S. H. Wan, J. B. Pu, L. P. Wang and X. Q. Liu, *J. Mater. Chem.*, 2011, **21**, 12251–12258.

14 J. B. Pu, S. H. Wan, G. A. Zhang, L. P. Wang, X. Q. Zhang, and Q. J. Xue, *J. Am. Chem Soc.,* 2013, **1**, 1254–1260.

15 Y. Zhou, Q. Bao, L. A. L. Tang, Y. Zhong and K. P. Loh, *Chem. Mater.*, 2009, **21**, 2950–2956.

16 A. A. Balandin, S. Ghosh, W. Z. Bao, I. Calizo, D. Teweldebrhan, F. Miao and X. N. Lau, *Nano letters*, 2008, **8**, 902–907.

17 J. U. Lee, D. Yoon, H. Kim, S. W. Lee and H. Cheong, *Phys. Rev. B,* 2011, **83**, 081419.

18 S. V. Morozov, K. S. Novoselov, M. I. Katsnelson, F. Schedin, D. C. Elias, J. A. Jaszczak and A. K. Geim, *Phys. Rev. Lett*, 2008, **100**, 016602.

19 K. I. Bolotin, K. J. Sikes, Z. Jiang, M. Klima and G. Fudenberg, *Solid State Commun.*, 2008, **146**, 351–355.

20 Z. Liu, J. Li, Z. Sun, G. Tai, S. Lau and F. Yan, *ACS Nano*, 2012, **6**, 810–818.

21 J. Zhang, P. Hu, X. Wang, Z. Wang, D. Liu, B. Yang and W. Cao, *J. Mater. Chem.*, 2012, **22**, 18283–18290.

22 J. Wu, M. Agrawal, H. A. Becerril, Z. N. Bao, Y. A. Chen and P. Peumans, *ACS nano*, 2009, **4**, 43–48.

23 A. Kasry, M. A. Kuroda, G. J. Martyna, G. S. Tulevski and A. A. Bol, *ACS nano*, 2010, **4**, 3839–3844.

24 X. Wang, L. Zhi and K. Mullen, *Nano Lett.*, 2008, **8**, 323–327.

25 S. P. Koenig, N. G. Boddeti, M. L. Dunn and J. S. Bunch, *Nat. Nanotechnology.*, 2011, **6**, 543–546.

26 C. Lee, X. D. Wei, J. W. Kysar and J. Hone, *Science*, 2008, **321**, 385–388.

27 H. Q. Chen, M. B. Müller, K. J. Gilmore,G. G. Wallace and D. Li, *Adv. Mater.*, 2008, **20**, 3557–3561.

28 I. W. Frank, D. M. Tanenbaum, A. M. Van der Zande and P. M. McEuen, *J. Vac. Sci. Technol., B*, 2007, **25**, 2558–2561.

29 S. S. Chen, L. Brown, M. Levendorf, W. W. Cai, S. Y. Ju, J. Edgeworth , X. S. Li, C. W. Magnuson, A. Velamakanni, R. D. Piner, J. Y. Kang and J. Park, *ACS Nano*, 2011, **5**, 1321–1327.

30 C. H. Chang, T. C. Huang, C. W. Peng, T. C. Yeh, H. I. Lu, W. I. Hung, C. J. Weng, T. I. Yang and J. M. Yeh, *Carbon*, 2012, **50**, 5044–5051.

31 R. S. K. Raman, P. C. Banerjee, D. E. Lobo, H. Gullapalli, M. Sumandasa, A. Kumar, L. Choudhary, R. Tkacz, P. M. Ajayan and M. Majumder, *Carbon*, 2012, **50**, 4040–4045.

32 D. Kang, J. Y. Kwon, H. Cho, J. H. Sim, H. S. wang, C. S. Kim, Y. J. Kim, R. S. Ruoff and H. S. Shin, *ACS Nano*, 2012, **6**, 7763–7769.

33 N. T. Kirkland, T. Schiller, N. Medhekar and N. Birbilis, *Corros Sci*, 2012, **56**, 1–4.

34 G. T. Kim, S. J. Gim, S. M. Cho, N. Koratkar and Il. Kwon Oh, *Adv. Mater.*, 2014, **26**, 5166–5172.

35 D. Prasai, J. C. Tuberquia, R. R. Harl, G. K. Jennings and K. I. Bolotin, *ACS Nano*, 2012, **6**, 1102–1108.

36 B. P. Singh, S. Nayak, K. K. Nanda, B. K. Jena, S. Bhattacharjee and L. Besra, *Carbon*, 2013, **61,** 47–56.

37 R. K. S. Singh, P. C. Chakraborty, D. E. Lobo, H. Gullapalli, M. Sumandasa, A. Kumar, L. Choudhary, R. Tkacz, P. M. Ajayan and M. Majumder, *Carbon* , 2012, **50**, 4040–4045.

38 B. P. Singh, B. K. Jena, S. Bhattacharjee and L. Besra, *Surf. Coat. Technol.*, 2013, **232**, 475–481.

39 Y. D Zhao, Y. Z Xie, Y. Y Hui, L. B Tang, W. J Jie, Y. F Jiang and Y. Chai, *J. Mater. Chem. C*, 2013, **1**, 4956–4961.

40 W. He, L. Zhu, H. Chen, H. Nan, W. Li, H. Liu, and Y. Wang, *Appl. Surf. Sci*, 2013, **279**, 416–423.

41 S. Mayavan, T. Siva and S. Sathiyanarayanan, *RSC Advances*, 2013, **3**, 24868–24871.

42 K. C. Chang, M. H. Hsu, H. I. Lu, M. C. Lai, P. J. Liu, C. H. Hsu, W. F. Ji, T. L. Chuang, Y. Wei, J. M. Yeh and W. R. Liu, *Carbon*, 2014, **66**, 144–153.

43 D. A. C. Brownson, L. J. Munro, D. K. Kampouis and C. E. Banks, *RSC Adv.,* 2011, **1**, 978–988

44 D. Chen, L. H. Tang and J. H. Li, *Chem. Soc. Rev.*, 2010, **39**, 3157–3180.

45 H. Bi, J. Chen, W. Zhao, S. R. Sun, Y. F. Tang, T. Q. Lin, F. Q. Huang, X. D. Zhou, X. M. Xie and M. Jiang, *RSC Adv.*, 2013, **3**, 8454–8460

46 M. Qian, A. M. Soutar, X. H. Tan, X. T. Zeng and S. L. Wijesinghe, *Thin Solid Films*, 2009, **517**, 5237–5242.

47 S. G. Chen, Y. Chen, Y. H. Lei, Y. S. Yin, *Electrochem. Commun.*, 2009, **11**, 1675–1679.

Figures caption

Fig. 1. SEM image of GO coating on Al alloy substrate.

Fig. 2. Schematic representation of preparation of superhydrophobic graphene and its coating on the Al alloy

Fig. 3. The CAs of graphene films prepared by different solvents and the shapes of water droplet on Al alloy surfaces; the water drops of as-prepared superhydrophobic graphene coatings on Al alloy under tilt angle of 0 and 180 in inset.

Fig. 4. XPS analysis of different samples and the C1s spectrum.

Fig. 5. FTIR spectrum of GO powder and graphene-E powder.

Fig. 6. AFM images of Graphene-E coating.

Fig. 7. The SEM photographs of different worn surfaces. (a) bare Al alloy. (b) graphene-coated Al alloy.

Fig. 8. Tafel plots of Bare Al alloy and Gr/Al samples. Best fits are represented by dotted lines.

Fig. 9. Nyquist plot of graphene coated Al alloy and bare Al alloy (a) and magnification of one segment (b).

Fig. 10. (a) Bode modulus diagrams and (b) Bode Phase angle diagrams of graphene coated Al alloy and bare Al alloy.

Fig. 11. The EEC employed to simulate the impedance data of the bare Al alloy substrate (a) and Al alloy coated with superhydrophobic graphene coating (b).

Fig. 12. Schematic of the corrosion mechanism occurring on bare Al alloy (a) and graphene coated Al alloy specimens (b).

407 Table 1. The results of corrosion test of the different samples in 3.5 wt.% NaCl
408 solution.
409

Sample	E_{corr}（V）	i_{corr}(A/cm^2)
Bare Al alloy	**-1.452**	**7.19×10^{-4}**
Gr/Al	**-1.329**	**2.54×10^{-7}**

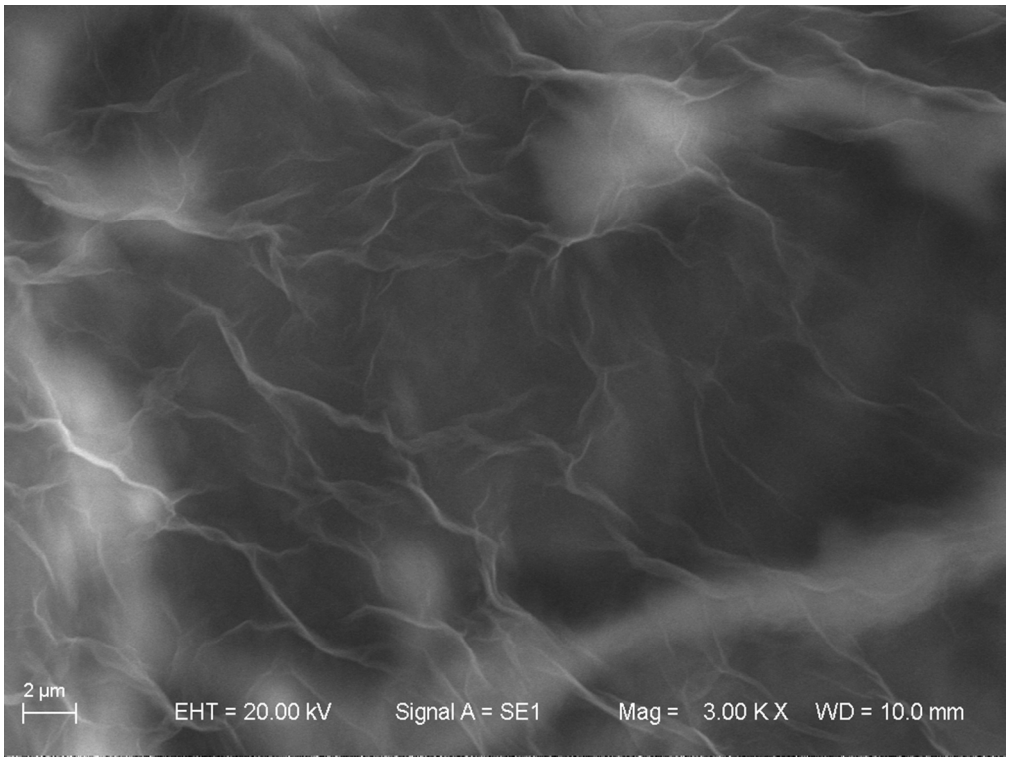

Fig. 1. SEM image of GO coating on Al alloy substrate.
26009x19507mm (1 x 1 DPI)

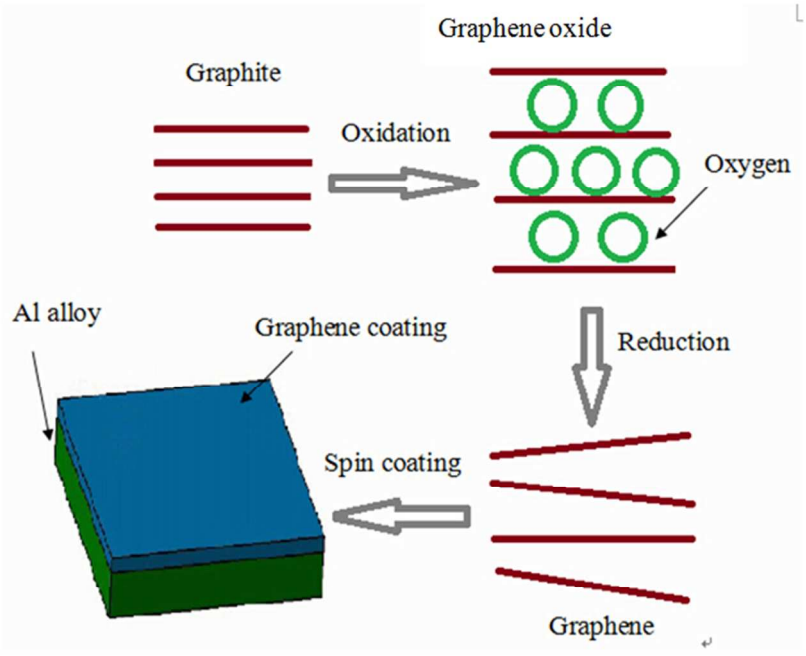

Fig. 2. Schematic representation of preparation of superhydrophobic graphene and its coating on the Al alloy
203x162mm (96 x 96 DPI)

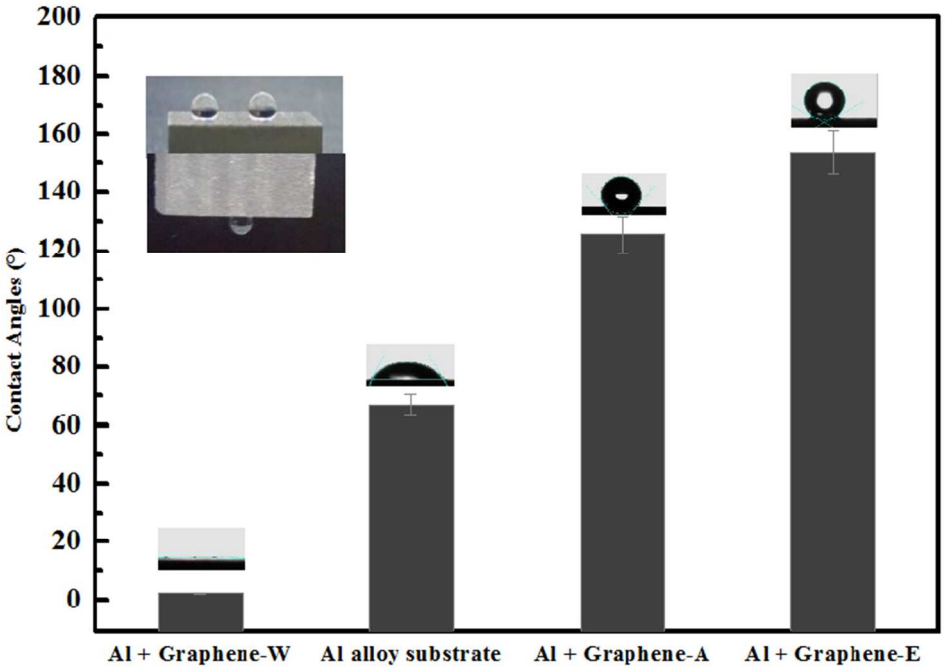

Fig. 3. The CAs of graphene films prepared by different solvents and the shapes of water droplet on Al alloy surfaces; the water drops of as-prepared superhydrophobic graphene coatings on Al alloy under tilt angle of 0 and 180 in inset.
216x165mm (96 x 96 DPI)

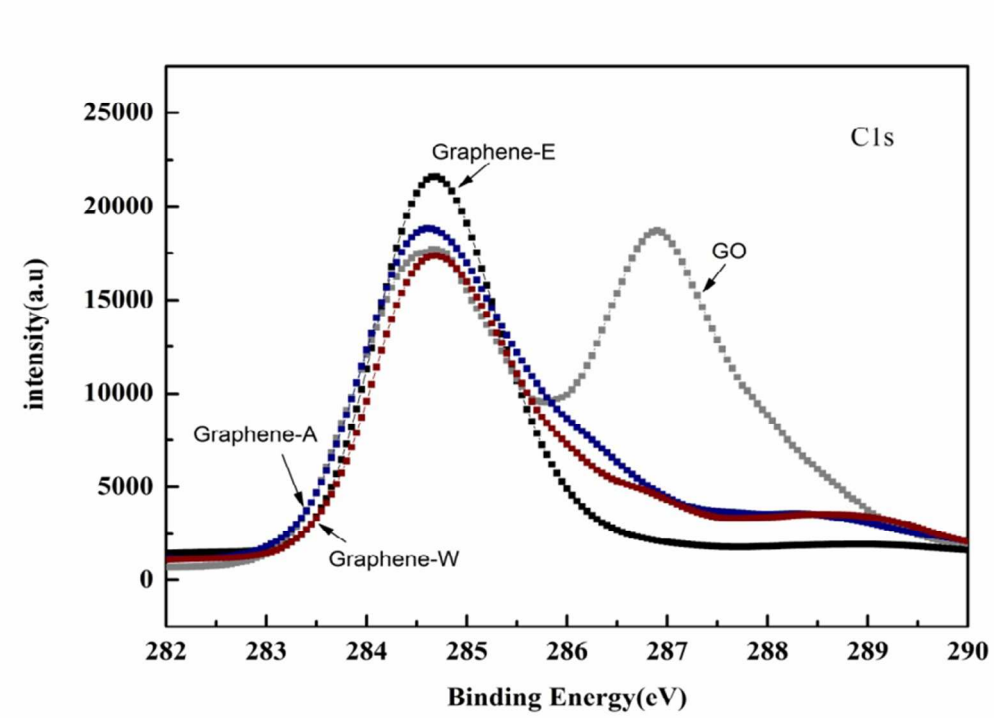

Fig. 4. XPS analysis of different samples and the C1s spectrum.
237x177mm (96 x 96 DPI)

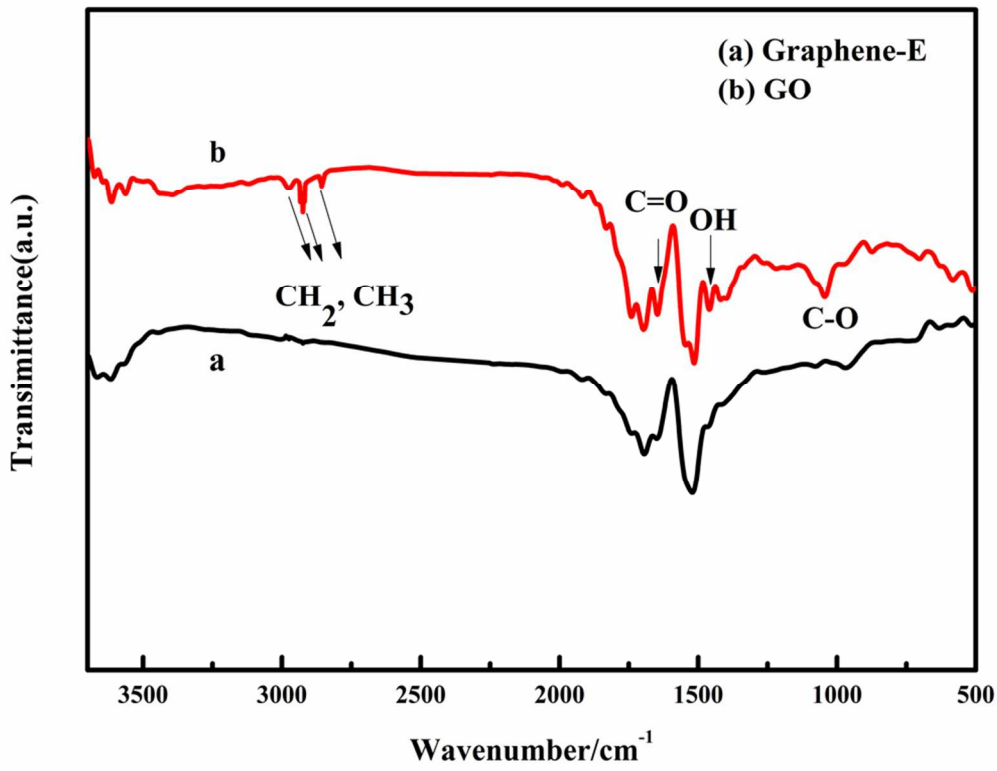

Fig. 5. FTIR spectrum of GO powder and graphene-E powder.
262x203mm (96 x 96 DPI)

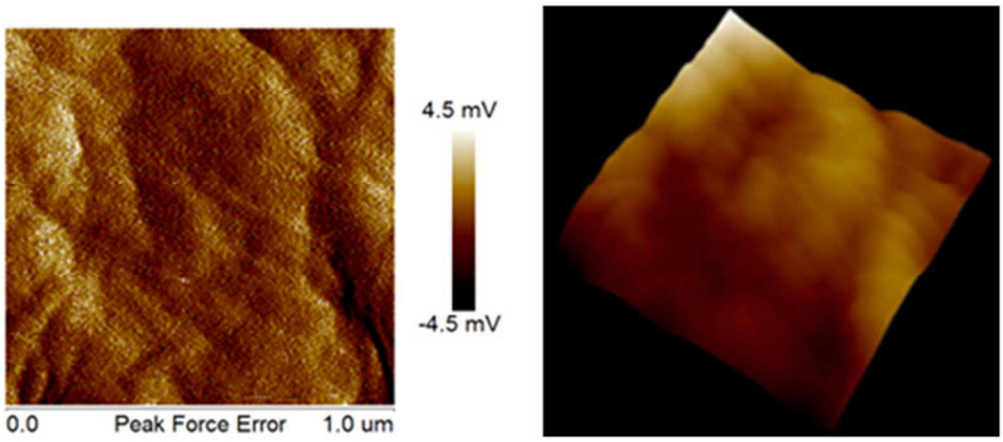

Fig. 6. AFM images of Graphene-E coating.
154x70mm (96 x 96 DPI)

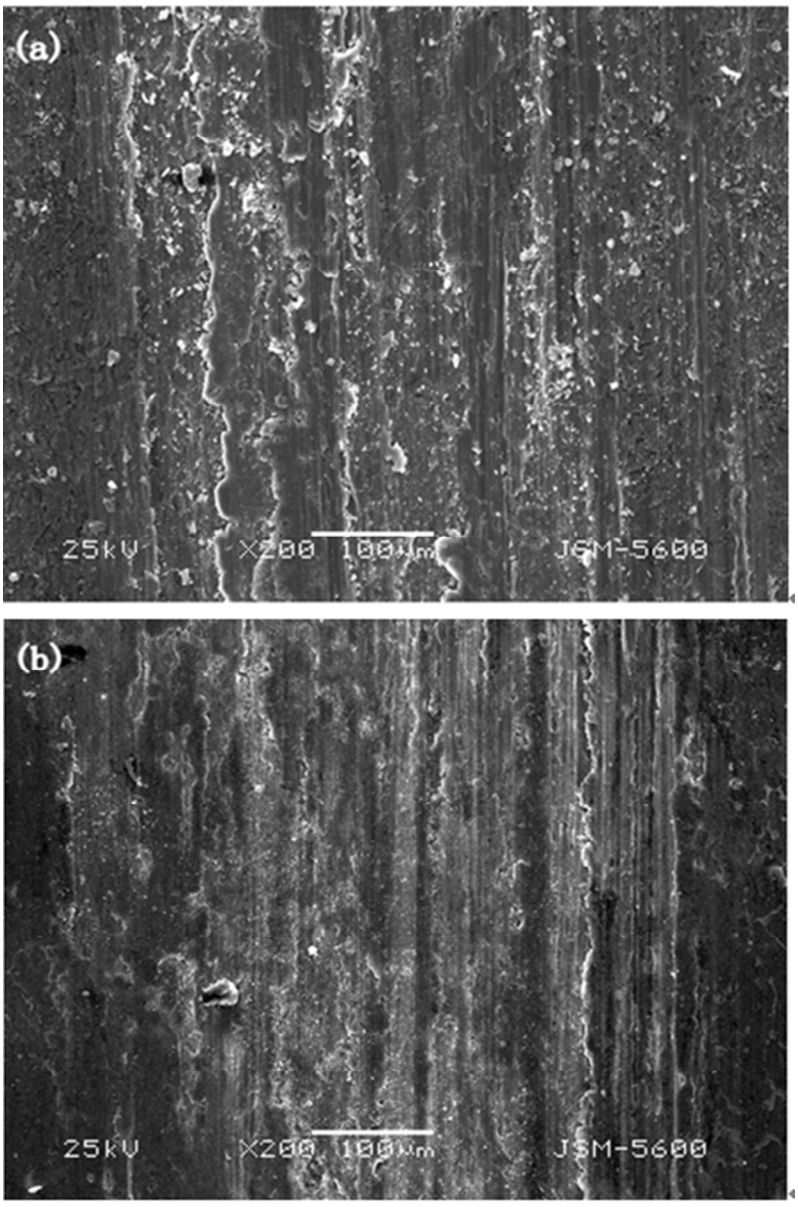

Fig. 7. The SEM photographs of different worn surfaces. (a) bare Al alloy. (b) graphene-coated Al alloy.
118x179mm (96 x 96 DPI)

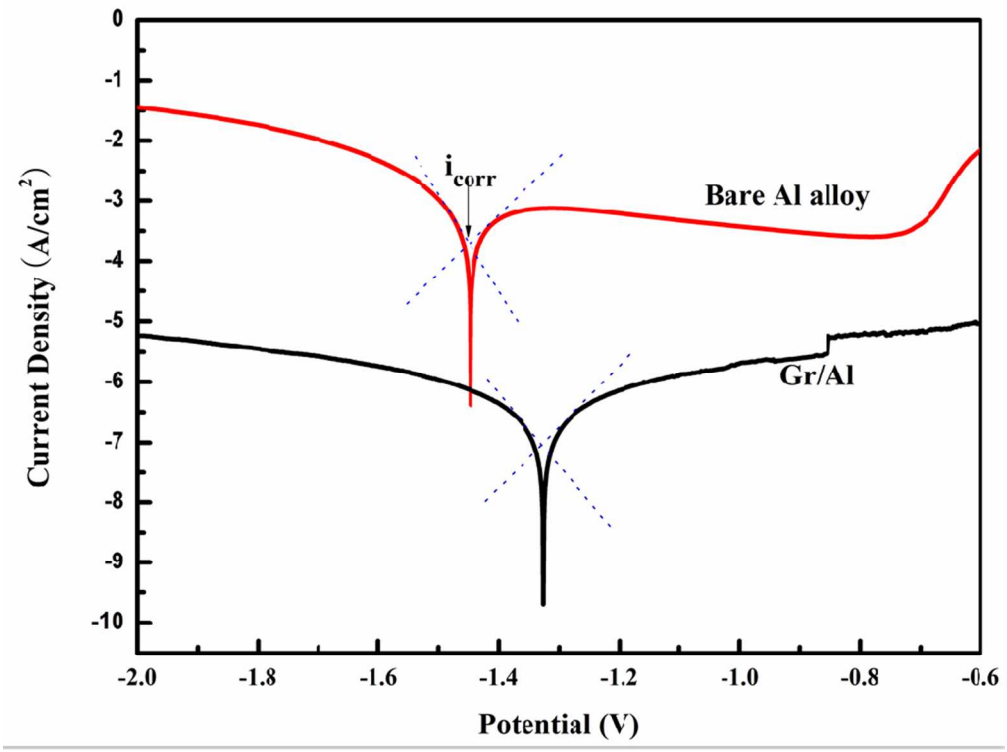

Fig. 8. Tafel plots of Bare Al alloy and Gr/Al samples. Best fits are represented by dotted lines.
268x201mm (96 x 96 DPI)

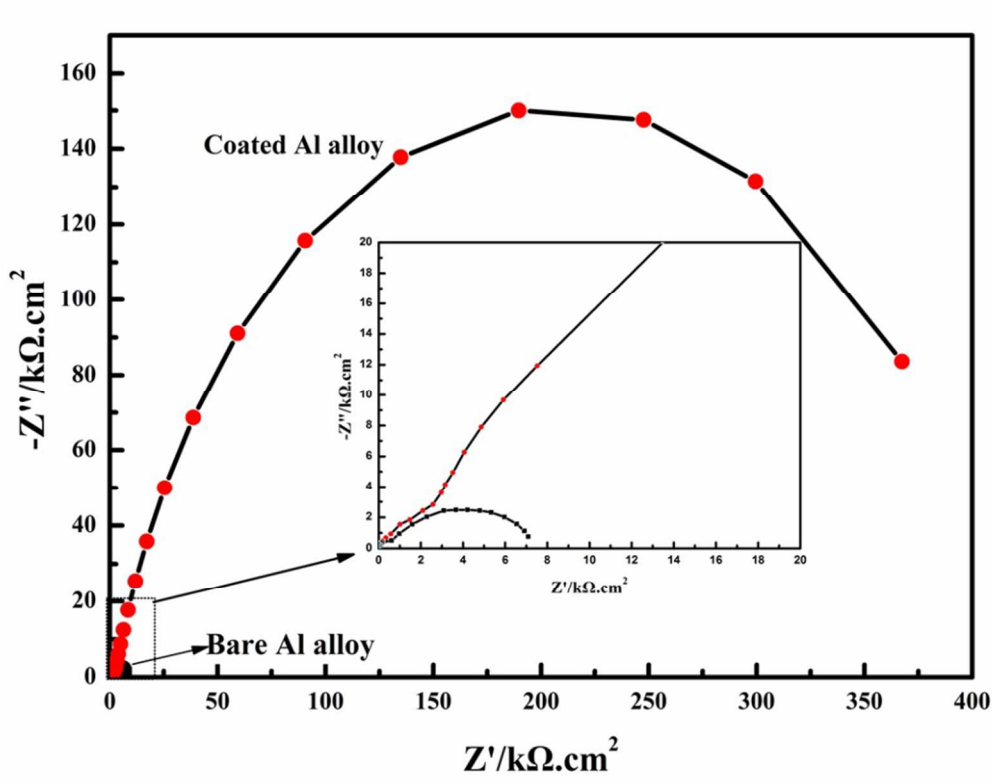

Fig. 9. Nyquist plot of graphene coated Al alloy and bare Al alloy (a) and magnification of one segment (b).
268x210mm (96 x 96 DPI)

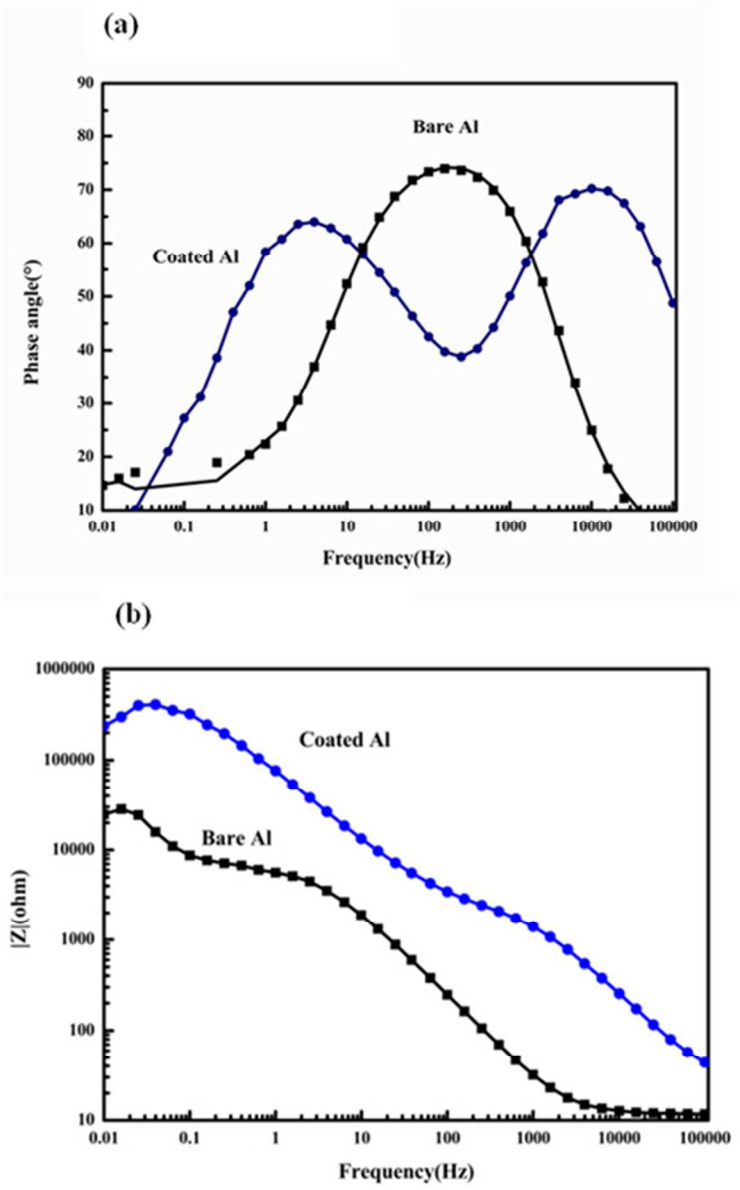

Fig. 10. (a) Bode modulus diagrams and (b) Bode Phase angle diagrams of graphene coated Al alloy and bare Al alloy.
125x199mm (96 x 96 DPI)

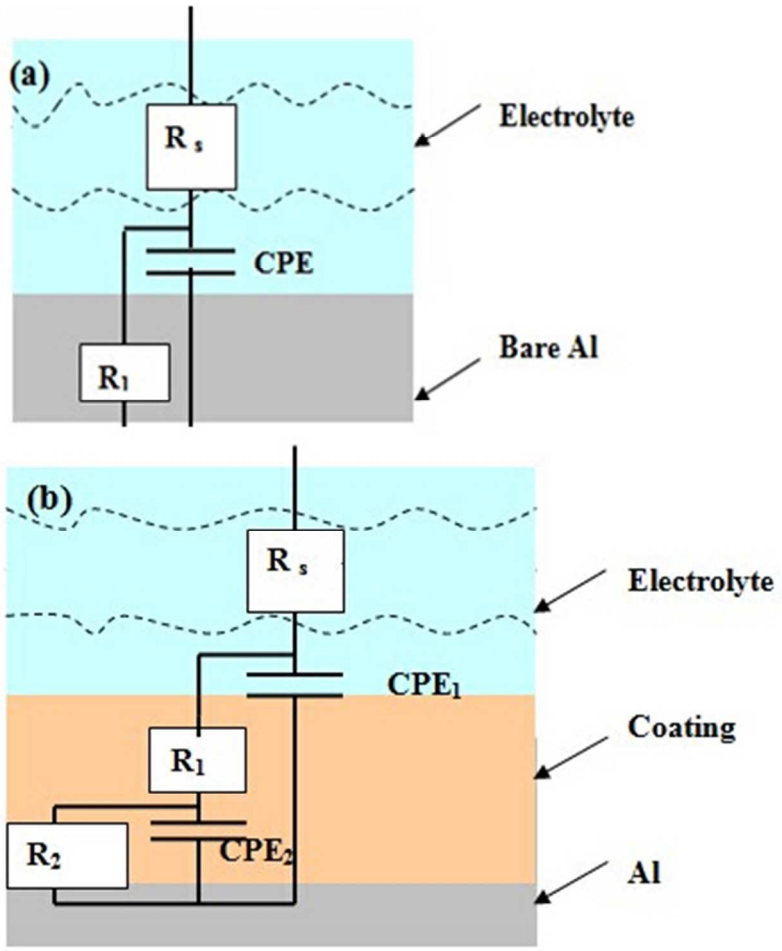

Fig. 11. The EEC employed to simulate the impedance data of the bare Al alloy substrate (a) and Al alloy coated with superhydrophobic graphene coating (b).
107x138mm (96 x 96 DPI)

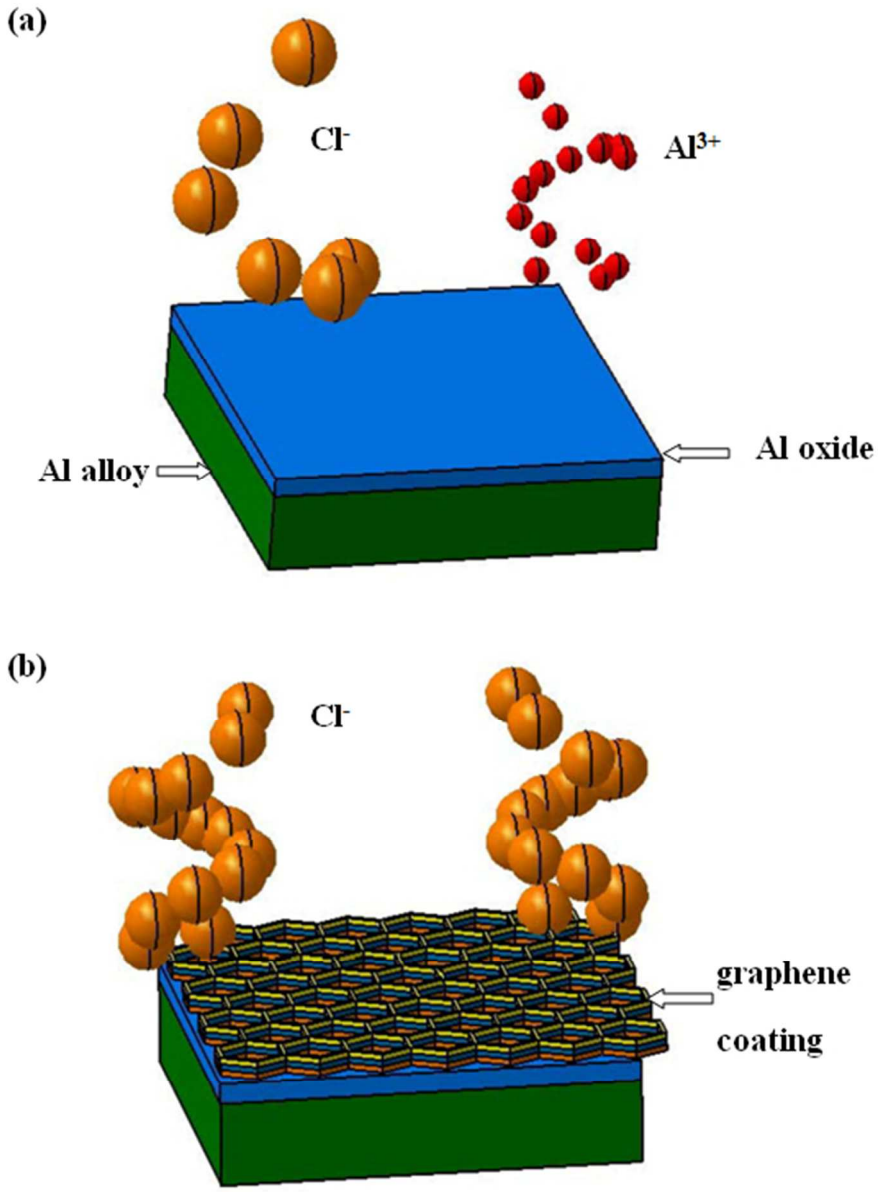

Fig. 12. Schematic of the corrosion mechanism occurring on bare Al alloy (a) and graphene coated Al alloy specimens (b).
143x194mm (96 x 96 DPI)